Photocatalytic Degradation of Methylene Blue Dye by Using Different Nanoparticles

Benazir S Pirjade[1], Shivaji Dinkar Jadhav[2], Israr Ahmad Shaikh[2], Sher Afghan Khan[3,*]

1   Bharati Vidyapeeth (Deemed to be University) Yashwantrao Mohite College of Arts, Science and Commerce, Pune-411038, India
2   Bharati Vidyapeeth (Deemed to be University) College of Engineering Pune -411043, India
3   Department of Mechanical Engineering, Faculty of Engineering, IIUM, Gombak Campus, Kuala Lumpur, Malaysia

ARTICLE INFO	ABSTRACT
	Zinc sulfide nanoparticles (NPs) were produced through a straightforward and cost-efficient chemical co-precipitation technique, intended for use in the photocatalytic decomposition of methylene blue (MB) dye, both under ultraviolet and visible light exposure. To evaluate the synthesized nanoparticles, various analytical tools including ultraviolet-visible (UV-Vis) spectroscopy, scanning electron microscopy (SEM), transmission electron microscopy (TEM), and X-ray diffractometry (XRD) were employed. The XRD analysis confirmed the cubic symmetry of the synthesized NPs. SEM analysis revealed that the nanoparticles tend to aggregate, forming clusters of nanoparticles. TEM analysis illustrated that the ZnS nanoparticles exhibit a spherical morphology with uniform size distribution. Additionally, Fourier-transform infrared (FTIR) analysis exhibited a vibrational peak at 616 cm $^{-1}$. The degradation of methyl blue was investigated using a UV-Vis spectrophotometer as part of the study.

1. Introduction

The importance of creating efficient and sustainable wastewater treatment techniques today cannot be emphasized, with environmental issues taking center stage in scientific and cultural debates. Synthetic dyes are one of the numerous toxins that pose a serious risk to aquatic ecosystems and human health. Textile, pharmaceutical, and paper industries all utilize these colors extensively [1]. Methylene blue (MB), a dye infamous for its persistence and resistance to traditional treatment approaches, is one well-known example of such contaminants. As a result, there is a pressing need for creative and ecologically benign methods to lessen the effects of such contaminants. One interesting route is the use of photocatalytic techniques that make use of various nanoparticles [2].

Recently, the idea of photocatalysis, a chemical reaction sparked by photon absorption by semiconductor materials, has attracted interest as an effective and environmentally friendly way to remove organic contaminants from water [3]. As it examines the breakdown of the well-known

pollutant, MB dye, this introduction will dig into the principles of photocatalysis and the fascinating world of nanoparticles [4].

To create and then recombine electron-hole pairs, photons must first be absorbed by a semiconductor material, which is the basis of photocatalysis. The process is driven by this core mechanism, which creates extremely reactive hydroxyl ($\bullet$OH) radicals with outstanding oxidative properties that may successfully mineralize organic molecules [5]. Due to their adequate bandgap energies and photostability, semiconductors like zinc oxide (ZnO), zinc sulfide (ZnS), and titanium dioxide (TiO_2) have received a lot of attention in the field of photocatalysis [6].

However, the distance between photogenerated electron-hole pairs and the catalyst's surface area has a significant impact on photocatalysis's effectiveness. The inclusion of nanoparticles is crucial at this point. Nanoparticles offer an abundance of active sites for accelerating photocatalytic processes because of their extraordinarily high surface area-to-volume ratio [7]. Additionally, due to their small size, they may effectively separate electron-hole pairs, reducing the chance of recombination and increasing the activity of the photocatalyst. Due to this special property, numerous nanoparticle kinds are being investigated as co-catalysts in photocatalytic systems meant to degrade MB dye. These include carbon-based nanoparticles, metal nanoparticles, and nanoparticles made of metal oxide [8].

Numerous aspects support the adaptability of nanoparticle selection in photocatalytic processes. When coupled with semiconductors, noble metal nanoparticles like gold (Au) and silver (Ag) have demonstrated astounding photocatalytic capabilities [9]. Due to their localized surface plasmon resonance (LSPR), these nanoparticles can absorb light in the visible spectrum, unlike most semiconductors, further increasing their usefulness. Additionally, some metals have special electrical properties that make charge transfer processes easier, increasing the effectiveness of dye degradation overall [10].

ZnS is one example of a metal sulfide nanoparticle that stands out for its stability and capacity to be customized in terms of size, shape, and crystal structure to suit a variety of applications. Because of their characteristics, they make excellent photocatalytic candidates for the removal of MB dye and other pollutants [11]. Meanwhile, due to their high electrical conductivity, carbon-based nanoparticles like graphene and carbon nanotubes hasten electron transport processes, increasing photocatalytic performance [12].

Through doping with other elements, the properties of ZnS, a semiconductor, can be improved, further increasing the efficiency of photocatalytic materials. By adding more energy levels to the bandgap, this doping technique reduces the rate of recombination by effectively trapping photogenerated hole pairs [13]. ZnS nanoparticles are given optical and luminous capabilities by transition metal doping, which includes elements like Ni, Cu, Zr, Mn, Co, and Fe [14]. This expands the range and applications of ZnS nanoparticles. X-ray diffraction (XRD), transmission electron microscopy (TEM), and scanning electron microscopy (SEM) are common methods used to characterize synthesized nanoparticles [15].

The ability of pure ZnS nanoparticles, Ni-doped ZnS nanoparticles, and Cu-doped ZnS nanoparticles to destroy methylene blue dye under various exposure times, both in the presence of UV and visible light, is evaluated as the photocatalytic efficacy of these materials [16].

2. Methodology
2.1 Synthesis

All of the chemicals utilized to make pure ZnS nanoparticles and doped ZnS nanoparticles were of analytical quality and required no additional purification before use. At room temperature, a

simple chemical co-precipitation approach was used to produce both pure ZnS nanoparticles and doped ZnS nanoparticles [17]. Precipitation of 0.1M zinc sulfide (0.8972gm of $ZnSO_4.H_2O$ in 50ml of deionized water) and 0.1M sodium sulfide (0.6604 gm of Na_2S in 50ml of deionized water) yielded the pure ZnS nanoparticles.

While stirring at 300 rpm, 0.1M zinc sulfide solution was added drop by drop from a burette containing 0.1M sodium sulfide solution. To regulate crystallinity, 1 g of PVP was added to the process as a capping agent with zinc sulfate.

Facilitates development and prevents clustering. After the process, a white precipitate developed. Two hours were spent agitating the solution at a steady rate of rotation. The reaction precipitate is collected and then centrifuged at 5000 rpm for 20 minutes to remove any remaining solids. Sonication is used to redisperse the ZnS nanoparticles that had settled to the bottom of the centrifuge tubes back into the deionized water. To get rid of any lingering contaminants or unreacted compounds, this procedure is done many times. Once the precipitate has been gathered, it is dried in a hot air oven. Then, using a mortar and pestle, they reduced the sample to a powder. Synthesis of zinc sulfide nanoparticles by chemical reaction

$$ZnSO_4 + Na_2S \rightarrow ZnS + Na_2SO_4 \qquad\qquad (1)$$
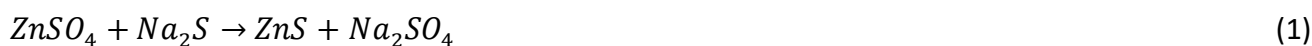
Zinc sulfide is doped with the salts of transition metals. For Ni-ZnS, $NiCl_2$, and Cu-ZnS, $CuSO_4$ is added along with zinc sulfide. All other stages of synthesis are unaltered.

2.2 Characterization

To meticulously conduct a thorough characterization of the synthesized Pure ZnS, Ni-doped ZnS, and Cu-doped ZnS nanoparticles, a variety of approaches were meticulously used [18]. First and foremost, the crystal structure of both undoped and doped ZnS nanoparticles was carefully examined using X-ray diffractometry (XRD). This in-depth investigation was carried out using a cutting-edge, Rikagu Ultima IV, X-ray diffractometer that was precisely operated at 40 kV and 40 mA with a wavelength of (λ=1.5406 A). The diffraction patterns that were recorded covered an extensive angular range 2θ, from 20º to a significant 80º.

At the same time, the morphological characteristics of these nanoparticles were painstakingly revealed by the clever use of Field Emission Scanning Electron Microscopy (FESEM). In this study, the cutting-edge, FEI Nova NanoSEM 450, device was skillfully used, enabling the collection of high-resolution morphological data of these nanoscale particles. Additionally, using Fourier-Transform Infrared (FT-IR) spectroscopy, a thorough evaluation of these nanoparticles' vibrational properties was methodically carried out.

Lastly, the optical absorption spectra were painstakingly recorded and examined using the state-of-the-art LABINDIA UV-3000 spectrophotometer, shedding light on the optical properties of the nanoparticles and their potential applications across the electromagnetic spectrum. These spectra covered a broad spectral range from 200 to a significant 800 nm.

2.3 Photocatalytic Degradation

The degradation of methylene blue dye was carefully studied to determine the photocatalytic activity of both doped (Ni-ZnS and Cu-ZnS) and undoped (ZnS) nanoparticles under two different irradiation conditions: UV (27 watts) and visible (50 watts).

This experiment was conducted in a solution comprising 80 mg of ZnS, Ni-ZnS, and Cu-ZnS nanoparticle catalyst carefully mixed with 5 mg per ml of methylene blue dye (MB dye), assuring extensive dispersion through constant stirring. Approximately 4ml of the reaction mixture was painstakingly removed at predetermined intervals of 0, 30, 60, 90, 120, 150, and 180 minutes. These extracted materials were then put through a demanding centrifugation procedure that involved spinning at 5,000 revolutions per minute for 20 minutes.

A UV-visible spectrophotometer was used to examine the methylene blue dye degradation with extreme care and precision, giving a thorough evaluation of the changes in dye concentration over time and shedding light on the efficiency of the photocatalytic process under both ultraviolet and visible irradiation conditions.

2.3.1 Mechanism for photocatalytic degradation

When a semiconductor photocatalyst is exposed to high-energy UV irradiation photons, the photocatalytic degradation pathway starts [19]. These photons have energies above the semiconductor photocatalyst's band gap energy, which causes the material to produce electrons (e-) in the conduction band (CB) and holes (h+) in the valence band (VB), as shown by Eq. (2)

$$(ZnS) + hv \rightarrow e^-(CB) + h + (VB) \tag{2}$$

Several critical processes in the degradation process are started by these newly created charge carriers. Reactive oxygen species (O_2) are produced as a result of interactions between electrons in the conduction band and oxygen molecules (O_2), as shown by Eq. (3)

$$(e^-) + O_2 \rightarrow O_2 \tag{3}$$

Eq. (4) shows what happens when holes in the valence band simultaneously react with water molecules (H_2O) to produce hydroxyl radicals (OH) and protons (H+)

$$(h+) + H_2O \rightarrow OH + H + \tag{4}$$

Furthermore, when the semiconductor photocatalyst is doped with ions like Mn2+, the holes (h+) may also interact with the dopant ions, resulting in the creation of different oxidation states of manganese ions (Mnn+), as illustrated in Eq. (5)

$$(from\ doped\ ZnS) + h+ \rightarrow Mnn + \tag{5}$$

The significance of photo-generated charge carriers in promoting the photocatalytic destruction of target pollutants is highlighted by this complex mechanism.

2.3.2 Calculation of degradation rate

The photocatalytic degradation rate was subsequently calculated using the following formula

$$Degradation\ rate\ (\%) = \frac{(A_0 - A)}{A_0} * 100 \tag{6}$$

3. Results and Discussion

3.1 X-Ray Diffraction Analysis (XRD)

Figure 1 carefully illustrates the X-ray diffraction (XRD) patterns of pure, Cu-doped, and Ni-ZnS nanoparticles. With unique reflections corresponding to the Miller planes (111), (220), and (311) seen at 2θ of about 28.6º, 47.8º, and 56.6º, respectively, these patterns unambiguously show three well-defined peaks across all samples. Notably, the XRD examination conclusively demonstrated the cubic zinc blend structure present in all samples, confirming the crystalline nature of ZnS.

It's important to note that the addition of impurity atoms of Copper (Cu) and Nickel (Ni) to the ZnS crystal lattice structure did not result in any observable new peaks in the XRD patterns, confirming their seamless integration into the ZnS lattice [20]. In addition, there was a small broadening of the XRD peaks, which is a phenomenon brought on by the presence of nanoparticles. Notably, the action of the added metal impurities resulted in a small size reduction of the ZnS nanoparticles. The different ionic radii of various elements, where Zn^{2+}, Ni^{2+}, and Cu^{2+} ions possess radii of 0.74, 0.69, and 0.73 respectively, may be responsible for this phenomenon. The decreased ionic radius of Zn^{2+} in comparison to the dopants may be the cause of this size reduction.

The Debye-Scherrer formula was carefully used to obtain the average crystallite size

$$d = \frac{k\lambda}{\beta cos\theta} \qquad (7)$$

where d stands for the nanocrystals' diameter, k is a constant (with a value of about 0.9), λ stands for X-rays' wavelength (λ=1.54056Å), β is the full-width half maximum (FWHM), and θ is the Bragg's angle. This formula was carefully used to calculate the average crystallite size, which revealed a range of 3 nm, indicating the nanoscale nature of the synthesized materials.
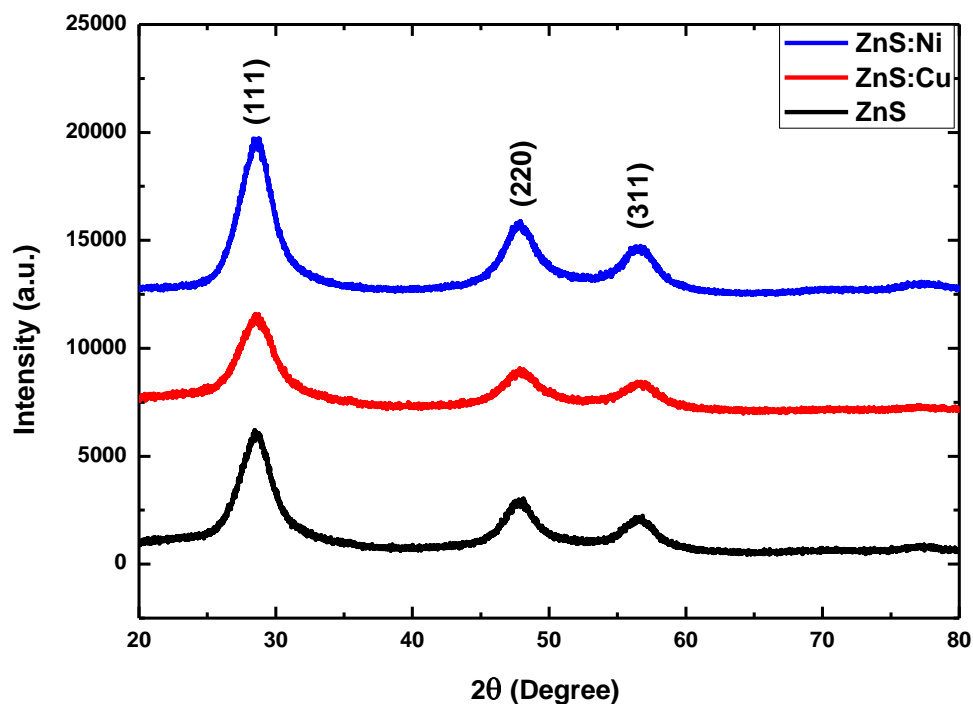

Fig. 1. XRD of ZnS, Cu-ZnS, and Ni-ZnS nanoparticles

3.2 Field Effect Scanning Electron Microscope (FESEM)

With the use of field effect scanning electron microscopy (FESEM), the morphology of both doped and undoped ZnS nanoparticles is shown in Figure 2(a), (b), and (c). These FESEM pictures, which are shown in the aforementioned figure, provide important information about the structural traits of the under-researched nanoparticles.
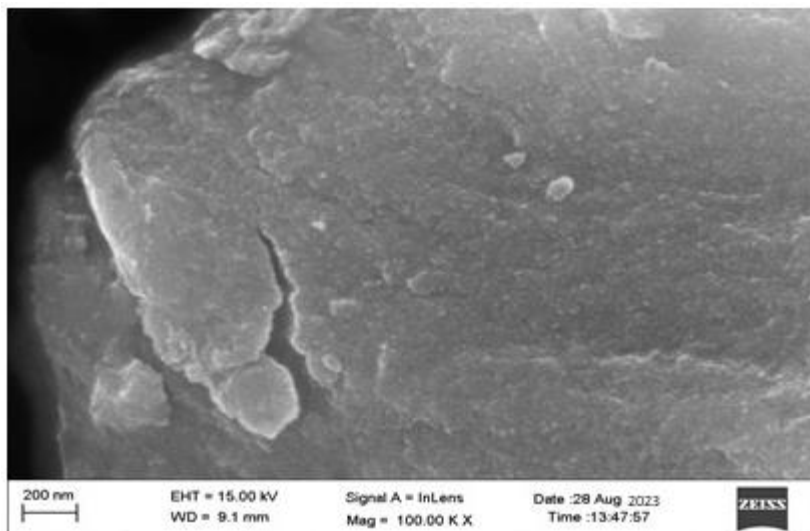
The pictures show the nanoparticle's size to be in the range of 30 nm in size. The diversity of the nanoparticle population is highlighted by this size difference, which is interesting given the possible effects it may have on various attributes and applications.
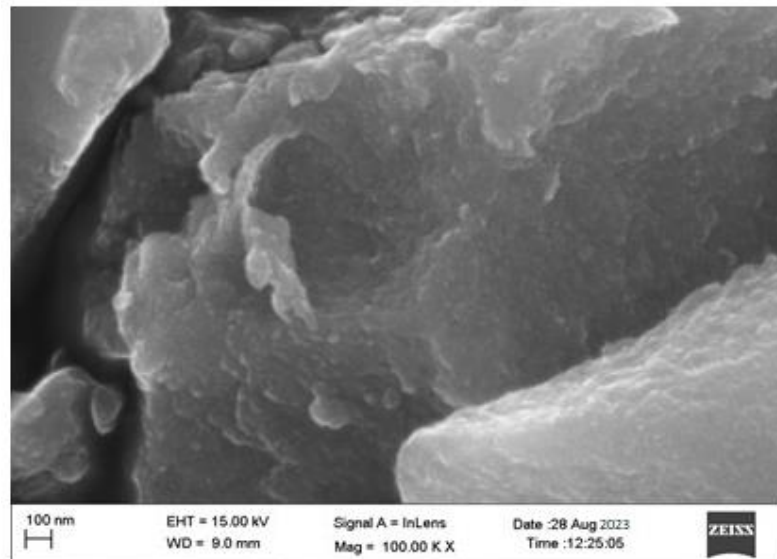
(a)
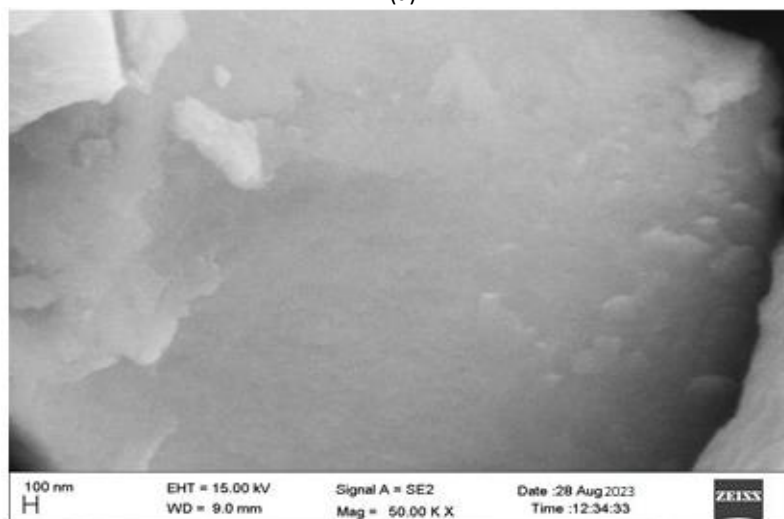
(b)

(c)

Fig. 2. SEM images of (a) Cu-Zns, (b) Ni-ZnS, (c) Pure ZnS

The SEM study revealed different morphologies for these nanoparticles, with spherical shapes and good size distribution. Notably, these nanoparticles have a propensity to group and create fascinating clusters and configurations. The intricacy of their possible applications and functional features is further increased by this aggregation process, which has a substantial impact on how they behave and interact in various settings.

3.3 Transmission Electron Microscopy (TEM)

The findings of a Transmission Electron Microscopy (TEM) investigation on both doped and undoped ZnS nanoparticles are shown in Figure 3. These TEM pictures provide crucial insights into the morphology and size of the nanoparticles by vividly illustrating their structural characteristics.

It is clear from the TEM pictures that the nanoparticles maintain an impressive level of size uniformity. A constant and well-defined spherical form dominates the detected nanoparticles. This consistency in both size and shape highlights the accuracy of the synthesis procedure and is an indication of the homogeneity attained in the population of nanoparticles.

Surprisingly, the TEM investigation conclusively determined that these nanoparticles' average size is only 3 nm. This nanoscale dimension is especially remarkable because it has important effects on the characteristics and prospective uses of nanoparticles, especially in areas like catalysis, sensing, and nanocomposite materials.
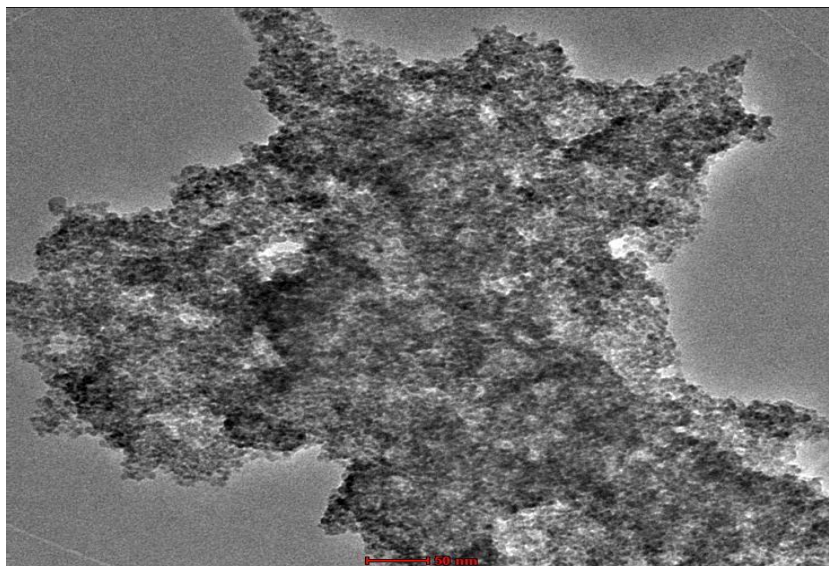
Fig. 3. TEM of nanoparticles

3.4 Fourier Transform Infrared Spectroscopy (FTIR)

To learn more about the composition of the nanocomposites made up of Ni-ZnS nanoparticles, Cu-ZnS nanocomposites, and virgin ZnS, we explore the Fourier-Transform Infrared (FTIR) spectra in Figure 4.

Intriguingly, a detailed examination of these spectra revealed unique peak wavenumbers in pure ZnS, N-ZnS nanoparticles, and Cu-ZnS nanocomposites, respectively, at 1071, 616, 576cm^{-1}. These different peaks act as definite markers of particular functional groups that are present in the materials. The peak at 1071 cm^{-1}, for instance, denotes the bending vibration of C-O bonds, while the peak at 616 cm^{-1} denotes the stretching vibration of Zn-S bonds. In addition, the peaks at 576cm^{-1} represent N-C=O. This thorough spectral analysis gives the materials under inquiry a precise molecular fingerprint that reveals information about their chemical makeup and structural characteristics.

A noteworthy finding from the FTIR spectra is that there don't seem to be any noticeable differences between the spectra of Cu-ZnS nanocomposites and Ni-ZnS nanoparticles. This modest fluctuation underlines the accuracy of the FTIR analysis in detecting even minute variances and draws attention to the intricacies in the chemical composition of these nanocomposites.

Furthermore, strain vibrations inherent to ZnS are captured in the FTIR spectrum at 616 cm^{-1}, adding to our knowledge of the material's structural features.
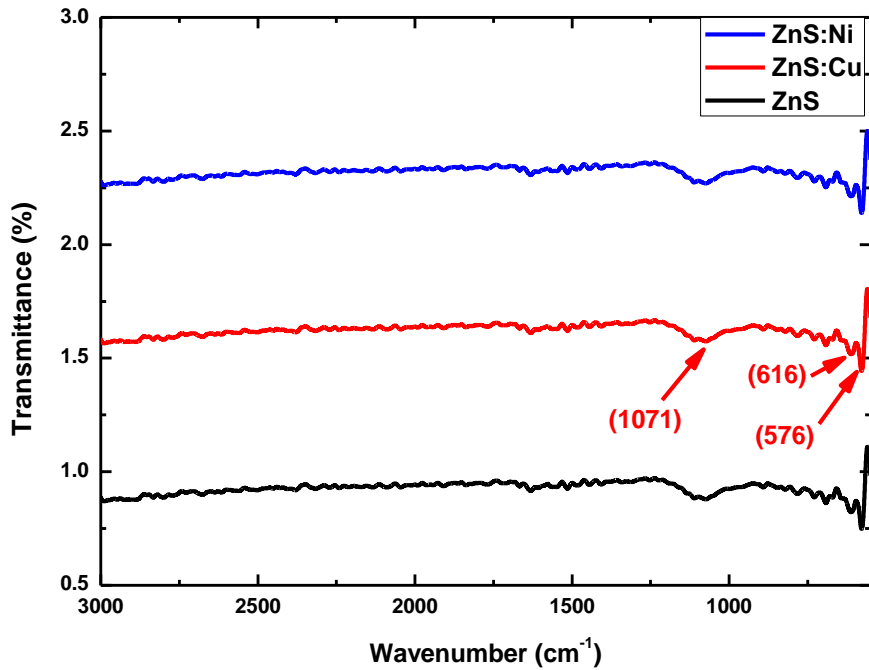
Fig. 4. FTIR analysis of ZnS, Cu-ZnS and Ni-ZnS nanoparticles

3.5 Optical Studies

Investigations into the optical characteristics of Pure ZnS, Ni-ZnS, and Cu-ZnS nanoparticles, as well as their related absorption spectra, have shown intriguing occurrences that merit careful study.

A noticeable and unique absorption edge conspicuously arises throughout the absorption spectra at 323 nm (refer to Figure 5). Notably, this edge changes slightly but noticeably towards the blue end of the spectrum when transition metals are injected. It's interesting to note that this shifting phenomenon does not appear to be significantly impacted by the specific sort of doping used. A distinctive feature of the quantum confinement effect, this shift in the absorption edge is a sign of significant changes in the electronic structure of the nanoparticles.
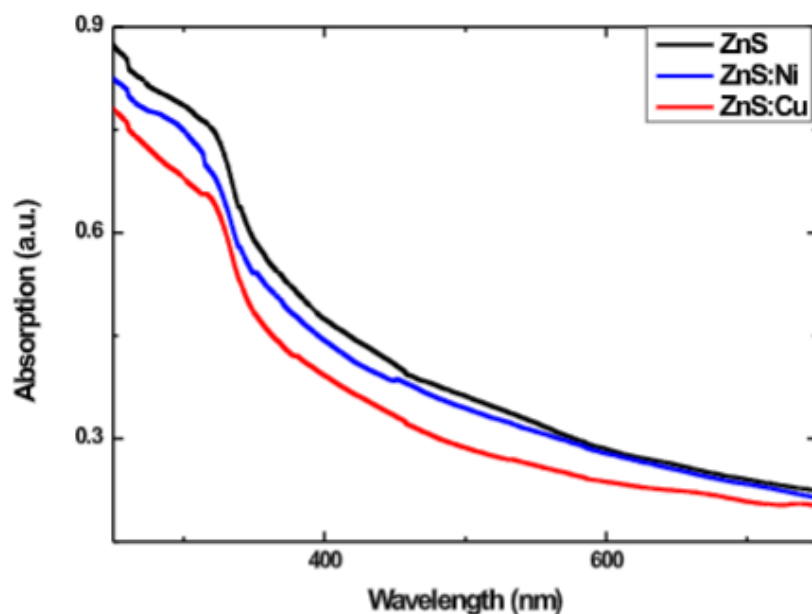

Fig. 5. UV visible spectra of ZnS, Ni-Zns, Cu-ZnS nanoparticles
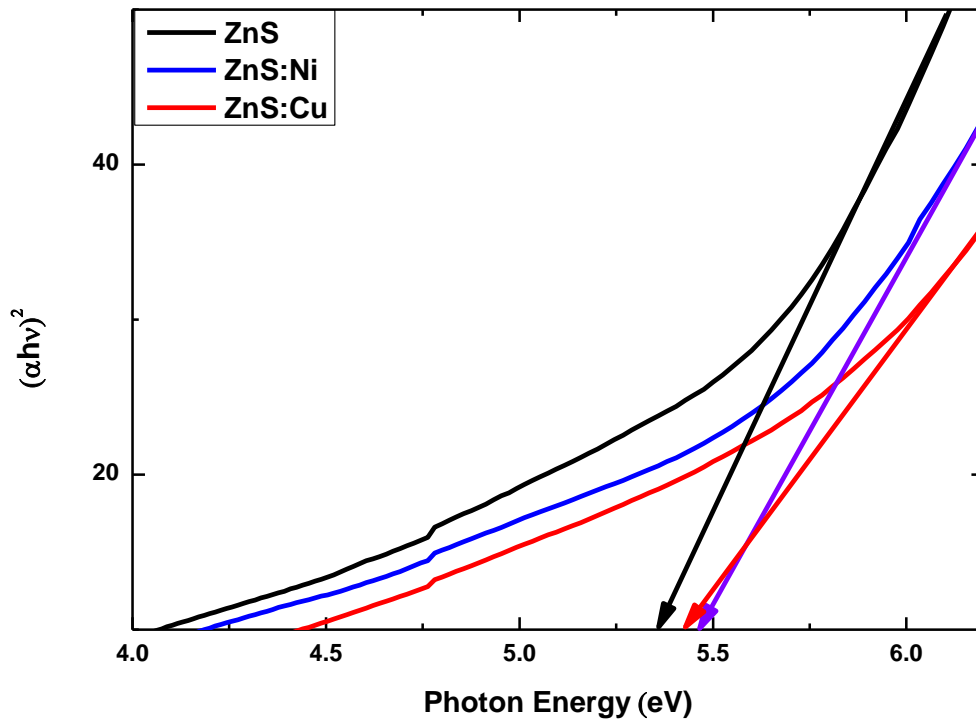
Fig. 6. Bandgap of ZnS, Ni-Zns, Cu-ZnS nanoparticles

A Tauc's plot method was skillfully used to quantitatively determine these changes in electrical characteristics, allowing the exact calculation of band gap values (refer to Figure 6). Surprisingly, this research showed that the band gap for pure Ni-ZnS nanoparticles was roughly 5.42 eV, whereas the band gap for Cu-ZnS nanoparticles showed a range extending from 5.46 eV. In sharp contrast to the bulk ZnS band gap of 5.36 eV, these computed band gap values provide evidence of the substantial influence of quantum confinement phenomena within the nanoparticles.

The application of a complex equation, as shown below, allowed for the derivation of nanoparticle size

$$E(r) = E_{bulk} + \frac{h^2}{8r^2}\left[\frac{1}{m_e^*} + \frac{1}{m_h^*}\right] - \frac{1.8e^2}{4\pi\varepsilon\,\varepsilon_0 r} \tag{8}$$

Where, E(r) in this equation stands for the band gap of the nanoparticles, whereas E$_{bulk}$ stands for the band gap of the bulk substance. The symbols for the effective masses of electrons and holes are m$_e$ and m$_h$, respectively. Though its effect is relatively small, it is significant that the third part of the equation includes an explanation for electron-hole attraction.

The diameter of the nanoparticles is approximated using this equation, and it turns out that they are about 3 nm in size. This dimension, which represents the significant influence of doping on nanoparticle dimensions and is probably influenced by quenching processes during the formation process, is particularly noteworthy. These discoveries highlight the fascinating potential of these materials across a range of industrial applications by shedding light on the complex interplay between material properties and quantum phenomena in the nanoscale domain.
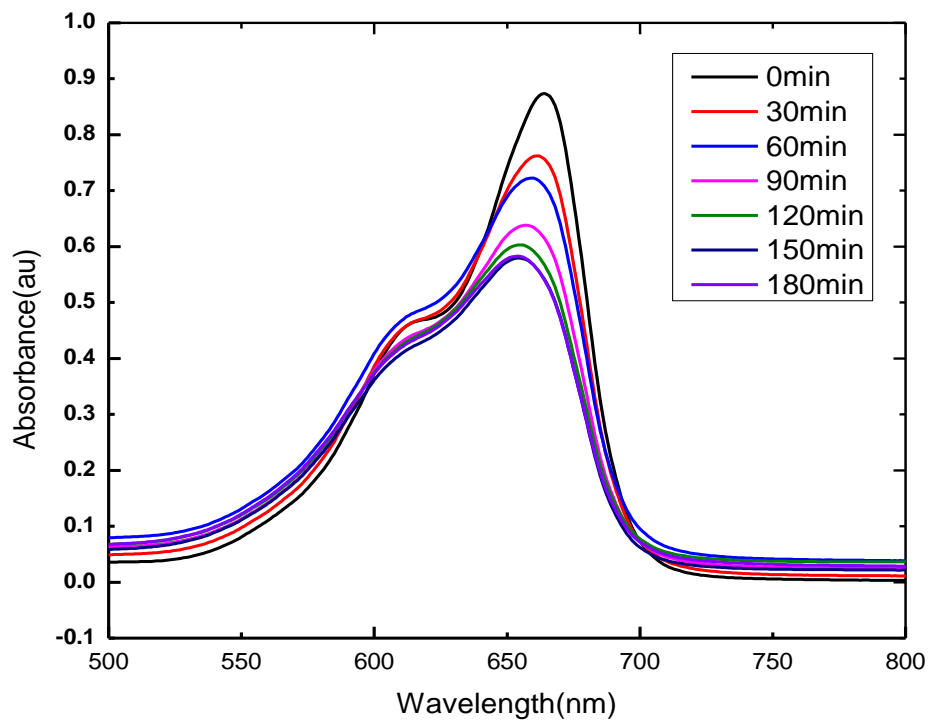
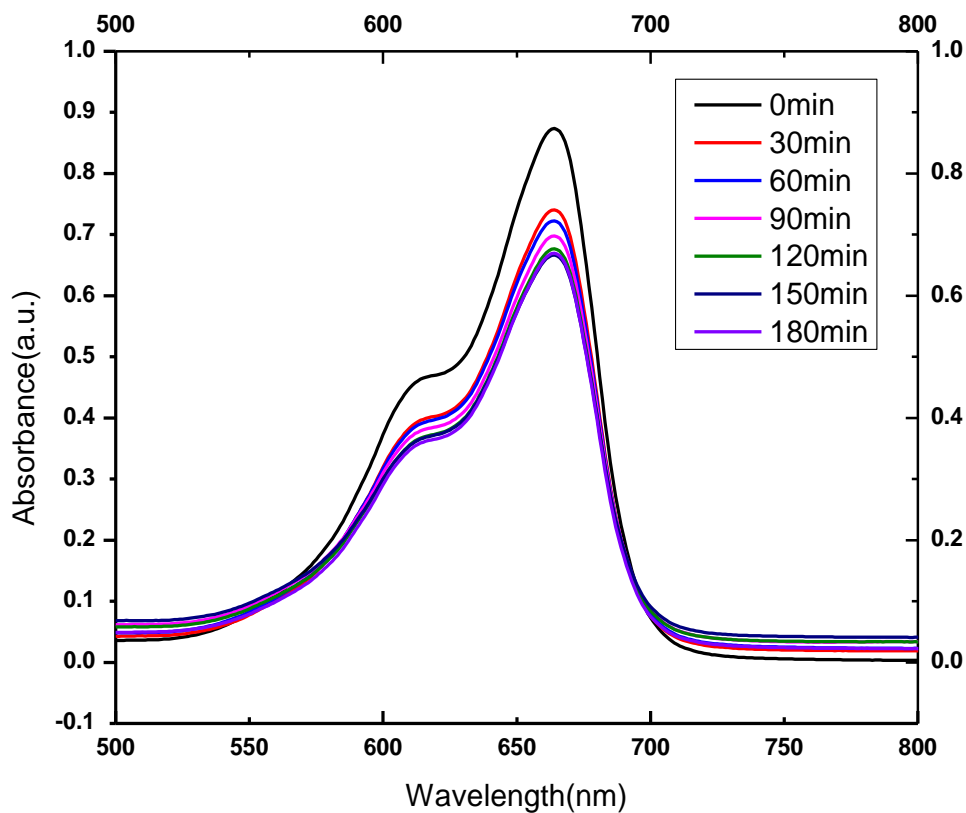**Fig. 7.** Photocatalytic degradation of Pure ZnS by UV

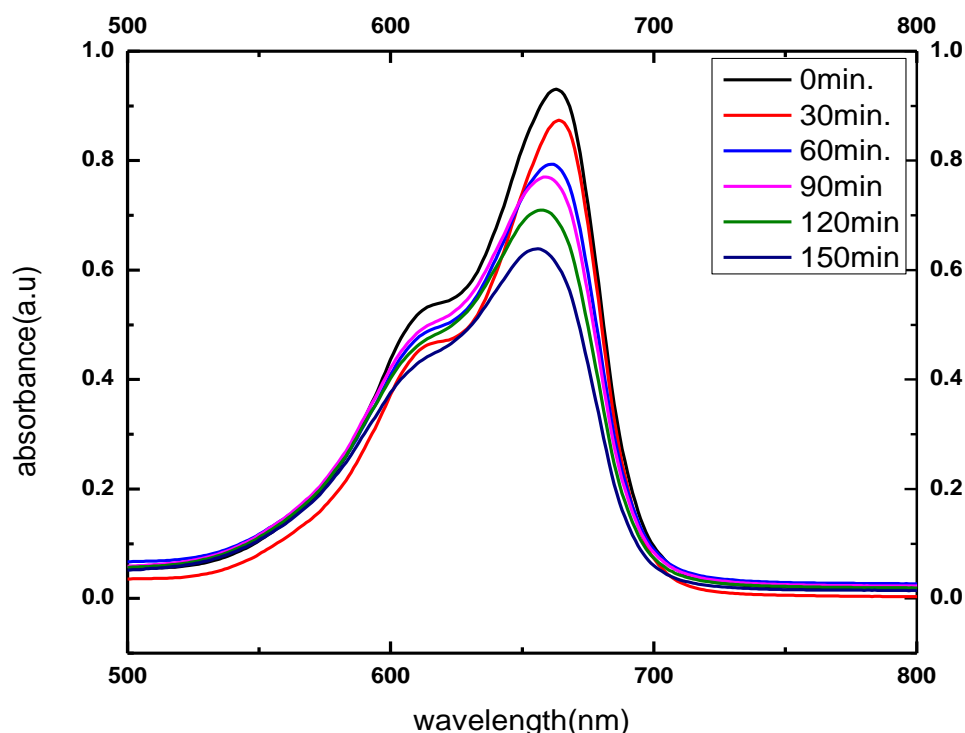**Fig. 8:** Photocatalytic degradation of Cu-ZnS by UV

Fig. 9. Photocatalytic degradation of Ni-ZnS by UV

The UV absorption spectra shown in Figures 7, 8, and 9 illustrate the photodegradation process for pure ZnS, Cu-ZnS, and Ni-ZnS, respectively. These spectra were taken at various time points. These spectra act as priceless diaries, providing a vivid depiction of the changing chemical changes taking place during the photodegradation process.

Intriguingly, more than just spectrum analysis has been used to explain the photocatalytic breakdown of methylene blue (MB) in the presence of all ZnS nanoparticles. It includes a thorough analysis of the corresponding photocatalytic degradation curves, illuminating the effectiveness of these nanoparticles in MB degradation.

These investigations revealed an interesting finding: all samples showed substantial MB degrading activity, above the 40% cutoff. Ni-ZnS nanoparticles displayed an exceptional degrading efficiency within the first 30 minutes of exposure, reaching a remarkable percent. The samples with dopants showed significant degradation efficiencies as well. Surprisingly, these three samples displayed a predictable pattern of behavior that closely matched the trends found in the photodegradation data.

These results highlight the amazing photocatalytic capacity of the synthesized nanoparticles, highlighting their efficiency in MB degradation and advancing our knowledge of their catalytic abilities.
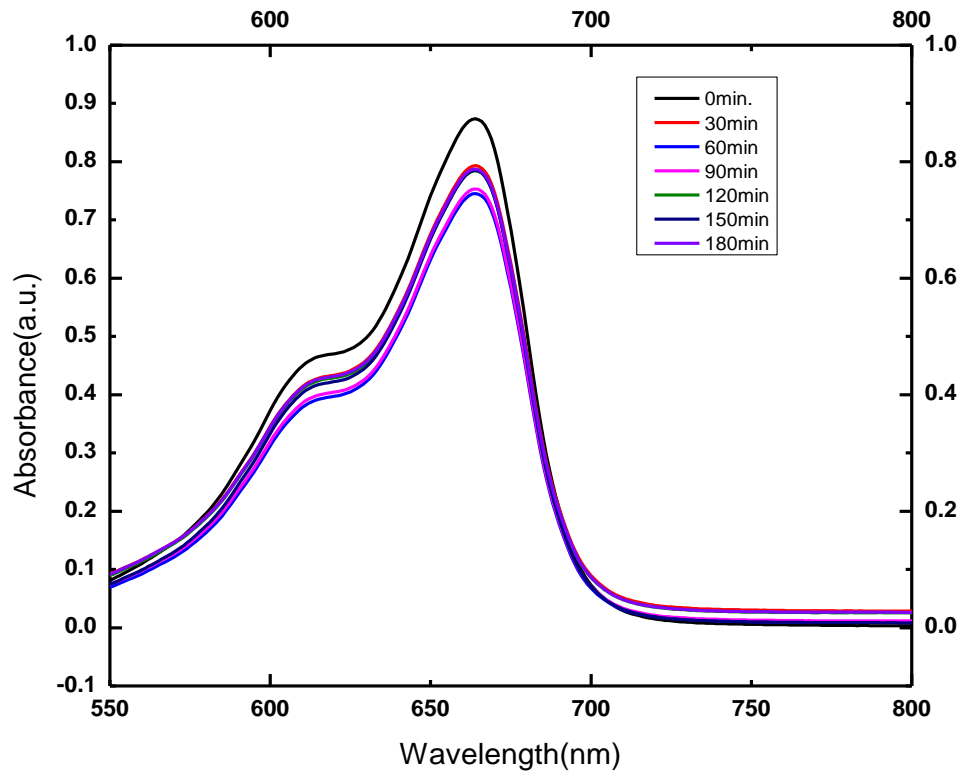
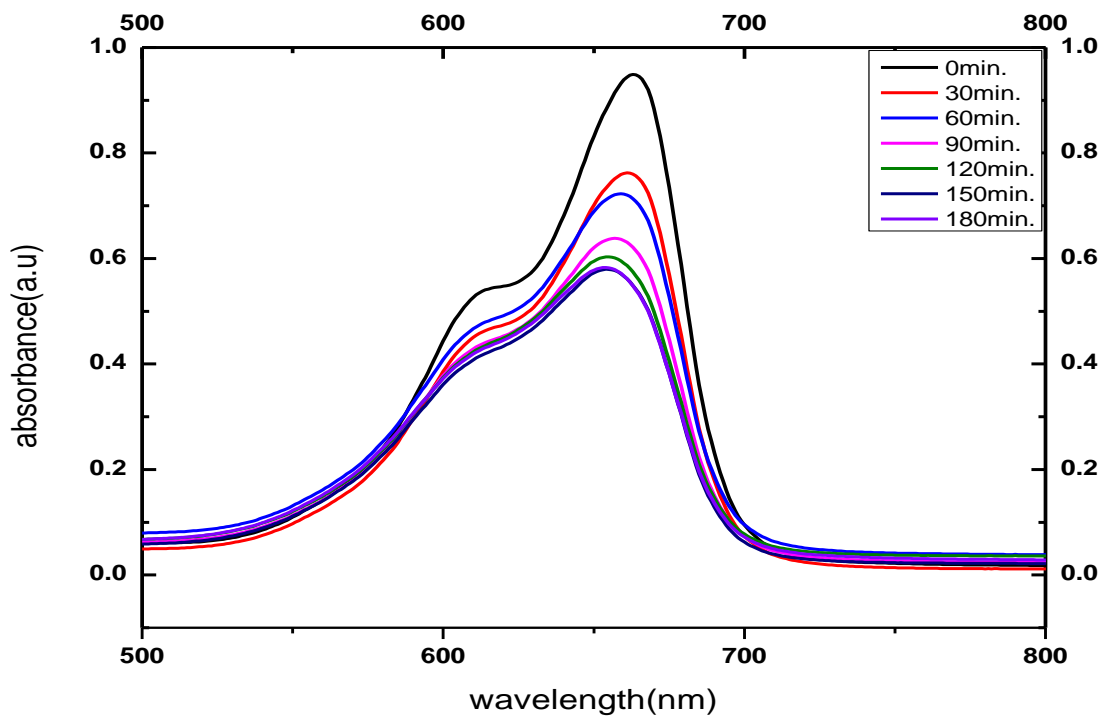**Fig. 10.** Photocatalytic degradation of Pure ZnS NP by visible irradiation

Fig. 11. Photocatalytic degradation of Cu-ZnS NP by visible irradiation
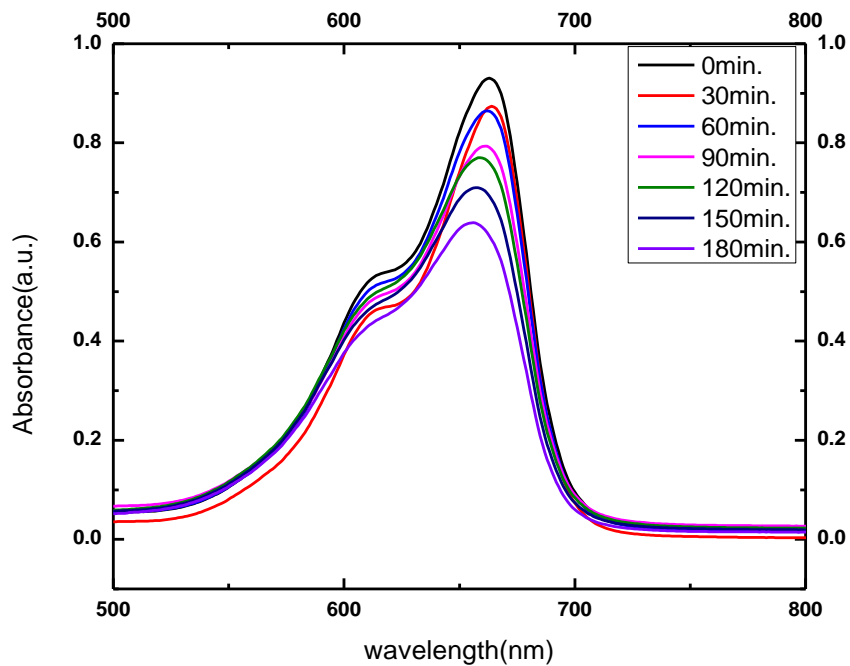
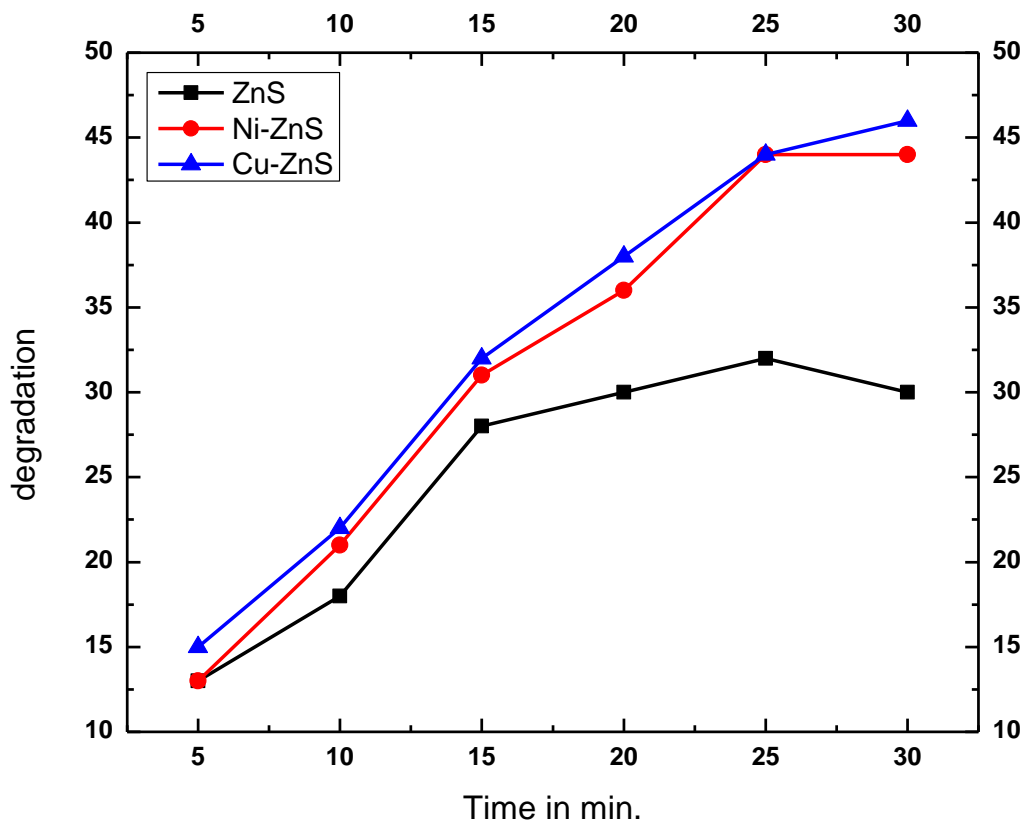**Fig. 12.** Photocatalytic degradation of Ni-ZnS NP by visible irradiation

Fig. 13. Photocatalytic degradation of MB dye in the presence of uv irradiation
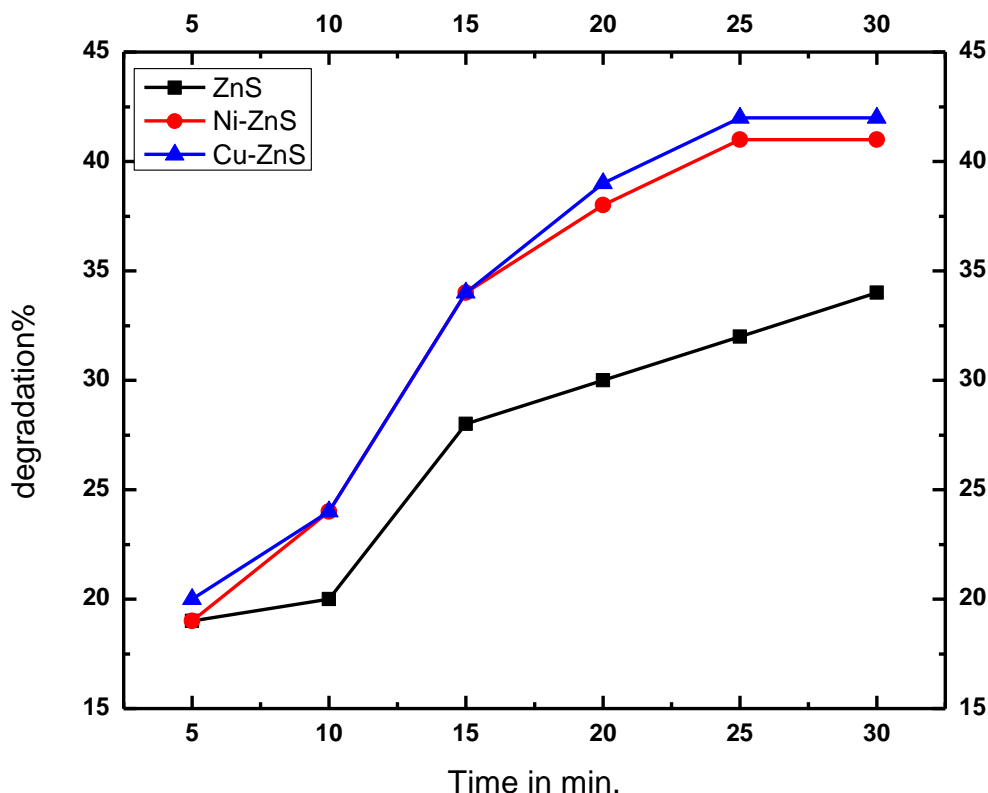
Fig. 14. Photocatalytic degradation of MB dye in the presence of visible irradiation

The absorption spectra for pure ZnS, Cu-ZnS, and Ni-ZnS nanoparticles, respectively, when exposed to visible light irradiation during varied periods ranging from 0 to 180 minutes, are comprehensively explored visually in Figures 10, 11, and 12. These spectrum representations offer priceless insights into the photodegradation mechanisms taking place inside these nanoparticles.

These spectra lead to an important finding since they unambiguously show the gradual photodegradation process. A noticeable decrease in absorption occurs as the exposure time increases, indicating the system's methylene blue (MB) dye is gradually deteriorating. The ongoing chemical reactions at work are captured by this dynamic shift in absorption spectra, providing an arresting visual account of the photodegradation process.

From Figures 13 and 14, it is clear that as uv and visible irradiation time increase percentage of degradation increases. Furthermore, a thorough analysis of the accompanying photocatalytic degradation performance results in a greater comprehension of the photocatalytic prowess of these nanoparticles in degrading MB. Surprisingly, the research shows that every sample showed strong MB degrading activity, exceeding the important 50% criterion. In this regard, it is interesting that doped ZnS nanoparticles demonstrated the best efficiency, than pure ZnS. These three samples, encouragingly, had a consistent behavioral pattern that closely mirrored the trends shown in the photodegradation data, supporting the consistency and repeatability of the reported photocatalytic effects.

These results advance our knowledge of the catalytic functions of the synthesized nanoparticles under visible light irradiation and reveal the remarkable photocatalytic abilities of the synthesized nanoparticles, making them ideal candidates for the effective degradation of MB.

4. Conclusion

Researchers can learn more about how nanoparticles, such as pure ZnS, Cu-ZnS, and Ni-ZnS, affect the photodegradation of the methylene blue (MB) dye by analyzing their absorption spectra when exposed to visible and UV radiation. A recurring pattern in the absorption spectra indicated the degradation of MB dye, showing a progressive decrease in absorption intensity over time, across various nanoparticles, and under various irradiation wavelengths. This declining absorption intensity correlates with continued exposure, demonstrating the efficiency of the photocatalytic process. With the help of these absorption spectra, different photocatalytic degradation curves can be derived, providing insight into how MB degrades when Cu/Ni-ZnS nanoparticles are present. These results show a linear decrease in absorption intensity with time, supporting the idea that Cu/Ni-ZnS nanoparticles have strong photocatalytic activity against the model dye pollutant MB. This in-depth study highlights the importance of photocatalysis based on nanomaterials in resolving the problems caused by organic dye pollution while emphasizing the potential of Ni-ZnS as a practical choice for photocatalytic degradation applications.

References

[1]   Tkaczyk, Angelika, Kamila Mitrowska, and Andrzej Posyniak. "Synthetic organic dyes as contaminants of the aquatic environment and their implications for ecosystems: A review." *Science of the total environment* 717 (2020): 137222. https://doi.org/10.1016/j.scitotenv.2020.137222

[2]   Moghaddas, Seyyed Mohammad Tabrizi Hafez, Behrouz Elahi, and Vahid Javanbakht. "Biosynthesis of pure zinc oxide nanoparticles using Quince seed mucilage for photocatalytic dye degradation." *Journal of Alloys and Compounds* 821 (2020): 153519. https://doi.org/10.1016/j.jallcom.2019.153519

[3]   Tian, Dongqi, Hongyu Zhou, Heng Zhang, Peng Zhou, Junjie You, Gang Yao, Zhicheng Pan, Yang Liu, and Bo Lai. "Heterogeneous photocatalyst-driven persulfate activation process under visible light irradiation: From basic catalyst design principles to novel enhancement strategies." *Chemical Engineering Journal* 428 (2022): 131166. https://doi.org/10.1016/j.cej.2021.131166

[4]   Chakraborty, Sonam, Nirman Chakraborty, Swastik Mondal, and Mrinal Pal. "Band gap engineered Sn-doped bismuth ferrite nanoparticles for visible light induced ultrafast methyl blue degradation." *Ceramics International* 48, no. 24 (2022): 37253-37263. https://doi.org/10.1016/j.ceramint.2022.08.303

[5]   Balu, Surendar, Chitiphon Chuaicham, Vellaichamy Balakumar, Saravanan Rajendran, Keiko Sasaki, Karthikeyan Sekar, and Arthanareeswari Maruthapillai. "Recent development on core-shell photo (electro) catalysts for elimination of organic compounds from pharmaceutical wastewater." *Chemosphere* 298 (2022): 134311. https://doi.org/10.1016/j.chemosphere.2022.134311

[6]   Karthikeyan, C., Prabhakarn Arunachalam, Kaliappan Ramachandran, Abdullah M. Al-Mayouf, and S. Karuppuchamy. "Recent advances in semiconductor metal oxides with enhanced methods for solar photocatalytic applications." *Journal of Alloys and Compounds* 828 (2020): 154281. https://doi.org/10.1016/j.jallcom.2020.154281

[7]   Iravani, Siavash, and Rajender S. Varma. "Sustainable synthesis of cobalt and cobalt oxide nanoparticles and their catalytic and biomedical applications." *Green Chemistry* 22, no. 9 (2020): 2643-2661. https://doi.org/10.1039/D0GC00885K

[8]   Qumar, Usman, Jahan Zeb Hassan, Rukhsar Ahmad Bhatti, Ali Raza, Ghazanfar Nazir, Walid Nabgan, and Muhammad Ikram. "Photocatalysis vs adsorption by metal oxide nanoparticles." *Journal of Materials Science & Technology* 131 (2022): 122-166. https://doi.org/10.1016/j.jmst.2022.05.020

[9]   Mondal, Kunal, and Ashutosh Sharma. "Recent advances in the synthesis and application of photocatalytic metal–metal oxide core–shell nanoparticles for environmental remediation and their recycling process." *RSC advances* 6, no. 87 (2016): 83589-83612. https://doi.org/10.1039/C6RA18102C

[10]   Koe, Weng Shin, Jing Wen Lee, Woon Chan Chong, Yean Ling Pang, and Lan Ching Sim. "An overview of photocatalytic degradation: photocatalysts, mechanisms, and development of photocatalytic membrane." *Environmental Science and Pollution Research* 27 (2020): 2522-2565.

https://doi.org/10.1007/s11356-019-07193-5

[11] Hassanpour, Mohammad, Hossein Safardoust-Hojaghan, and Masoud Salavati-Niasari. "Degradation of methylene blue and Rhodamine B as water pollutants via green synthesized Co3O4/ZnO nanocomposite." *Journal of Molecular Liquids* 229 (2017): 293-299. https://doi.org/10.1016/j.molliq.2016.12.090

[12] Feng, Chang, Zhuoyuan Chen, Jiangping Jing, Mengmeng Sun, Jing Tian, Guiying Lu, Li Ma, Xiangbo Li, and Jian Hou. "Significantly enhanced photocatalytic hydrogen production performance of g-C3N4/CNTs/CdZnS with carbon nanotubes as the electron mediators." *Journal of Materials Science & Technology* 80 (2021): 75-83. https://doi.org/10.1016/j.jmst.2020.11.047

[13] Jaiswal, R., N. Patel, D. C. Kothari, and Antonio Miotello. "Improved visible light photocatalytic activity of TiO2 co-doped with Vanadium and Nitrogen." *Applied Catalysis B: Environmental* 126 (2012): 47-54. https://doi.org/10.1016/j.apcatb.2012.06.030

[14] Azab, A. A., Ebtesam E. Ateia, and S. A. Esmail. "Comparative study on the physical properties of transition metal-doped (Co, Ni, Fe, and Mn) ZnO nanoparticles." *Applied Physics A* 124 (2018): 1-10. https://doi.org/10.1007/s00339-018-1871-3

[15] Jay Chithra, M., M. Sathya, and K. J. A. M. S. Pushpanathan. "Effect of pH on crystal size and photoluminescence property of ZnO nanoparticles prepared by chemical precipitation method." *Acta Metallurgica Sinica (English Letters)* 28 (2015): 394-404. https://doi.org/10.1007/s40195-015-0218-8

[16] Pascariu, Petronela, Ioan Valentin Tudose, Mirela Suchea, Emmanouel Koudoumas, Nicusor Fifere, and Anton Airinei. "Preparation and characterization of Ni, Co doped ZnO nanoparticles for photocatalytic applications." *Applied surface science* 448 (2018): 481-488. https://doi.org/10.1016/j.apsusc.2018.04.124

[17] Mittal, Manish, Manoj Sharma, and O. P. Pandey. "UV–Visible light induced photocatalytic studies of Cu doped ZnO nanoparticles prepared by co-precipitation method." *Solar Energy* 110 (2014): 386-397. https://doi.org/10.1016/j.solener.2014.09.026

[18] Shaili, Hamza, El mehdi Salmani, Rida Essajai, Mustapha Beraich, Wafaa Battal, Mouad Ouafi, Abderrahim Elhat et al. "Structural, electronic and optical properties of Cu-doped ZnS thin films deposited by the ultrasonic spray method-DFT study." *Optical and Quantum Electronics* 53, no. 6 (2021): 300. https://doi.org/10.1007/s11082-021-02934-8

[19] Sil, Devika, and Sampa Chakrabarti. "Photocatalytic degradation of PVC–ZnO composite film under tropical sunlight and artificial UV radiation: A comparative study." *Solar Energy* 84, no. 3 (2010): 476-485. https://doi.org/10.1016/j.solener.2009.09.012

[20] Mingos, D. Michael P. "Early history of x-ray crystallography." *21st Century Challenges in Chemical Crystallography I: History and Technical Developments* (2020): 1-41. https://doi.org/10.1007/430_2020_73